J Mater Sci (2007) 42:9983–9989
DOI 10.1007/s10853-007-2059-y

Microstructure and properties of Mg–5.6%Sn–4.4%Zn–2.1%Al alloy

S. Harosh · L. Miller · G. Levi · M. Bamberger

Received: 26 April 2007 / Accepted: 25 July 2007 / Published online: 6 September 2007

Abstract In a previous study, Mg–Sn–Zn-based alloys showed insufficient structural stability at elevated temperatures. In order to improve the castability and corrosion resistance 2.1%wt Al was added to the Mg–5.6%Sn–4.4%Zn base alloy. At the as-cast condition, SEM micrographs indicate a very fine microstructure (Dendritic Arm Spacing—DAS—smaller than 17 μm). The study focuses on precipitation hardening, phase formation and structural stability, during the aging of solution treated samples at elevated temperatures. After solution treatment and aging at 225 °C, Vickers hardness measurements show that this alloy maintains a constant increase of 30% in hardness for periods of up to 32 days. EDS (SEM & STEM), XRD, and Auger characterization methods were applied to identify the phases presented in the alloy. There is no evidence for the presence of the deleterious γ-$Al_{12}Mg_{17}$ phase. SAXS measurement and STEM micrographs reveal very fine precipitations (less than 100 nm) after 32 days of aging, along with homogenously distributed larger precipitations (up to 500 nm).

Introduction

Magnesium alloys are known for their lightweight, high-specific stiffness, and very good castability and workability. Therefore, due to the demand for weight reduction of automotive components, the use of Mg alloys has significantly increased in recent years. A commercial alloy, such as AZ91, contains high amounts of Al and some Zn. Al improves the castability, corrosion resistance, and strength at room temperature, however, this alloy exhibits poor creep resistance at elevated temperatures [1–3]. The main reason for the poor creep resistance is the precipitation of the γ-$Mg_{17}Al_{12}$ phase at grain boundaries.

In order to exploit the positive effect of Al, while avoiding its harmful influence at elevated temperatures, it was decided to reduce the amount of Al to 2 wt%. Based on previous research [4, 5], the main alloying elements were chosen to be Zn and Sn. Zn has several benefits in Mg based alloys [6, 7]. It increases the creep resistance, and forms several stable intermetallic phases with Mg. At the eutectic temperature, 6.2%wt of Zn can be dissolved into Mg [8]. At room temperature, the maximum solubility drops to 2%wt. In a similar way, Mg can dissolve 14.6%wt Sn at the eutectic temperature [8]. Sn can form stable Mg_2Sn particles. During the aging of an Mg–Sn–Zn based alloy, firstly semi-coherent $MgZn_2$ particles precipitate, which later transform into an incoherent MgZn phase, and secondly Mg_2Sn precipitates are formed [5]. The precipitation mechanism is diffusion controlled. The precipitates are uniformly distributed in the Mg-matrix with two morphologies: needle- and plate–like shapes [4, 5]. However, limited structural stability during aging at 175 °C of the alloys investigated in [4, 5] was found, due to characteristic rapid precipitation.

The main goal of the current study was to investigate microstructural stability of the alloy Mg–Sn–Zn–Al, compared to the base alloy studied earlier: Mg–3.8%Sn–4.5%Zn. The investigated alloy was characterized in the as-cast, solution treated state, and after aging and exposure to 225 °C for up to 32 days. The precipitation hardening was studied by Vickers hardness measurements and the microstructure by XRD, SEM, STEM, SAXS, DSC and

S. Harosh · L. Miller · G. Levi · M. Bamberger (✉)
Department of Material Engineering, Technion IIT, Haifa 32000, Israel
e-mail: mtrbam@tx.technion.ac.il

Auger spectroscopy. In order to find the controlling mechanism in each precipitation stage, the activation energy of the process was calculated.

Material and experimental procedure

Melting and casting

Table 1 lists the composition of the alloy investigated in this research; Pure Magnesium of 99.98% and aluminum of 99.95% were melted in a cemented graphite crucible under protective atmosphere of 60cc/min CHF134A + 1 L/min CO_2 gas mixture. When the magnesium and aluminum were completely melted, 99.8% pure zinc and 99.95% pure Sn were added into the melt at about 720 °C. After 20 min, the melt was poured at a temperature of 720 °C into a steel disc shaped mold of 60 mm in diameter and 9 mm thick.

Solution treatment

Slices from the as-cast alloys were cut and encapsulated in quartz ampoules under 400 mm Hg Argon atmosphere, to prevent oxidation during solution treatment. The solution treatment was conducted in a Lindberg resistance furnace. This treatment included fast heating to 350 °C, holding for 48 h, and slow heating at a rate of 1 °C per hour up to 450 °C and holding at that temperature for additional 96 h. Finally the samples were quenched into water.

This solution treatment is aimed to ensure complete dissolution of the alloying elements in the α-Mg matrix without any grain boundary melting. The solution treatment temperature was based on thermodynamic calculations using the Thermo-Calc software package.

Precipitation hardening

Solution treated samples ($10 \times 10 \times 5$ mm^3) were put into a molten salt bath (sodium nitrate 50% and potassium nitrate 50%) at 225 °C for different time periods up to 32 days. The molten salt was stirred and temperature controlled to ensure uniform and stable temperature of the salt during the experiments. For the purpose of finding the activation energy in the investigated alloy, aging for 2 h at different temperatures ranging from 150 °C to 275 °C was carried out. At the end of treatment the samples were quenched in water.

Table 1 The chemical composition of the investigated alloy (determined by DIRATS Lab USA)

	Mg	Sn	Zn	Al
%Wt	87.9	5.6	4.4	2.1

Exposure to elevated temperatures

Samples ($10 \times 10 \times 5$ mm^3) in the as-cast state were put into the molten salt bath at 225 °C for different time periods up to 32 days. At the end of treatment the samples were quenched in water.

Characterization and measurements

Specimens for optical and electron microscopy were polished with a 320–1200 mesh papers and finally with an oil-based suspension of 0.05μm alumina. The samples' microstructure, morphology and chemistry were investigated by SEM, XRD, EDS, Auger, and SAXS. TEM investigation was also carried out on samples 20 nm thick in the center (after polishing, dimpling and PIPS). Microhardness measurements were conducted using the Vickers method (1 kg and 100 g loads), in order to monitor the precipitation strengthening process. DSC scans of samples in the as-cast state were taken for acquiring thermodynamic data and were compared with the calculated results.

Results

As-cast state

SEM micrograph taken from the first third of the specimens, perpendicular to the solidification direction of the investigated alloy is shown in Fig. 1.

The microstructure of the as-cast state consists of a dendritic α-Mg matrix (dark phase) with thick bright boundaries reflecting the high concentration of alloying elements at grain boundaries. Similar coring effect has

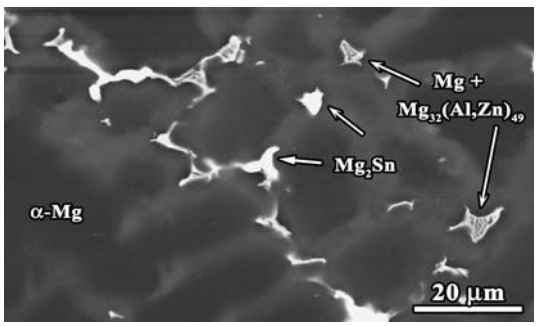

Fig. 1 SEM micrograph of the investigated alloy in as-cast condition

Table 2 Mean composition at grain boundaries and within the α-Mg matrix [%wt]

	α-Mg		At grain boundaries	
	Mean	Std	Mean	Std
Mg	93.9	0.7	88.1	1.6
Al	1.7	0.5	2.7	0.7
Zn	1.5	0.2	3.4	1.3
Sn	2.9	0.6	5.7	0.6

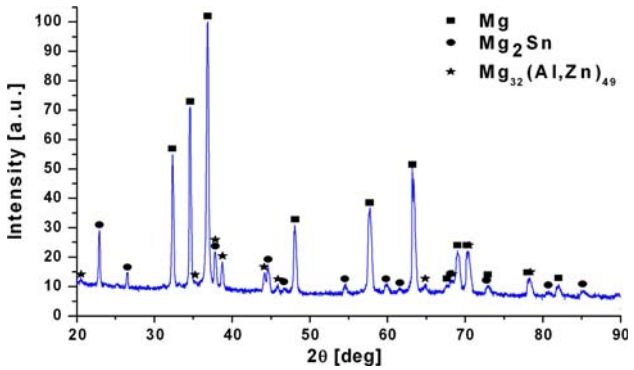

Fig. 2 X-ray diffraction spectra for the as-cast condition

been previously shown [4, 5]. The chemical composition (EDS measurements) of α-Mg phase and the gray area near grain boundaries are given in Table 2. This alloy shows a very fine morphology with DAS of 16.6 ± 3.5μm.

The alloy microstructure contains an Mg_2Sn phase and eutectic α-Mg + $Mg_{32}(Al,Zn)_{49}$ phase, which was verified by XRD (shown in Fig. 2) and TEM electron diffraction given in Fig. 3, as well compositional analysis utilizing STEM+EDS (Table 3). The presence of γ-$Mg_{17}Al_{12}$ could not be proven either by elements mapping by EDS, Auger analysis or by XRD.

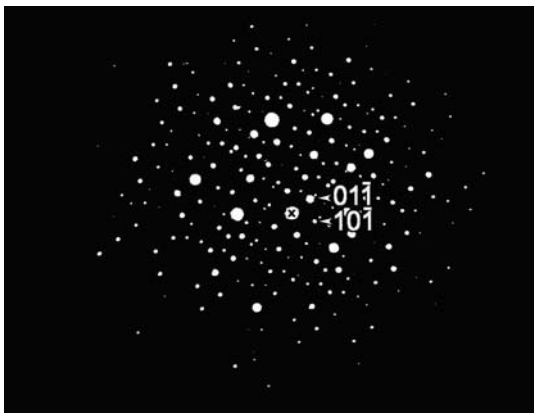

Fig. 3 Electron diffraction taken from zone axis [111] of $Mg_{32}(Al,Zn)_{49}$ phase. The transmitted beam is marked X. The pattern of the cubic $Mg_{32}(Al,Zn)_{49}$ precipitate (JCPDS19–29) is indexed

Table 3 Chemical composition of $Mg_{32}(Al,Zn)_{49}$ phase (%at)

	Mean	std
Mg	40.2	0.3
Al	16.2	0.3
Zn	43.6	0.4

Thermodynamic data of the investigated alloy was found by DSC scans at a heating rate of 10 °C /min (shown in Fig. 4). The melting temperature of each phase, noticeable by its characteristic endothermic peak, corresponds quite well with published data and Thermo-Calc calculations: 348 °C for the eutectic reaction, 563 °C of Mg_2Sn and 615 °C is the liquidus temperature. The total enthalpy of melting is 214.9J/g as against 246.1J/g calculated by Thermo-Calc software package.

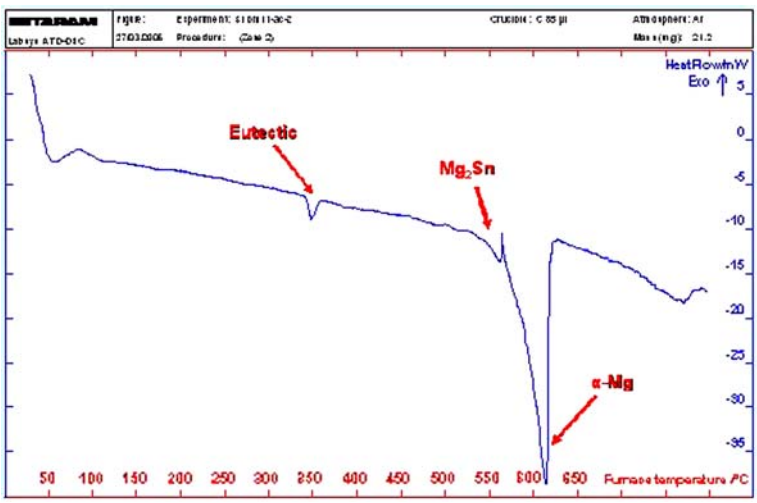

Fig. 4 DSC scan at as-cast condition

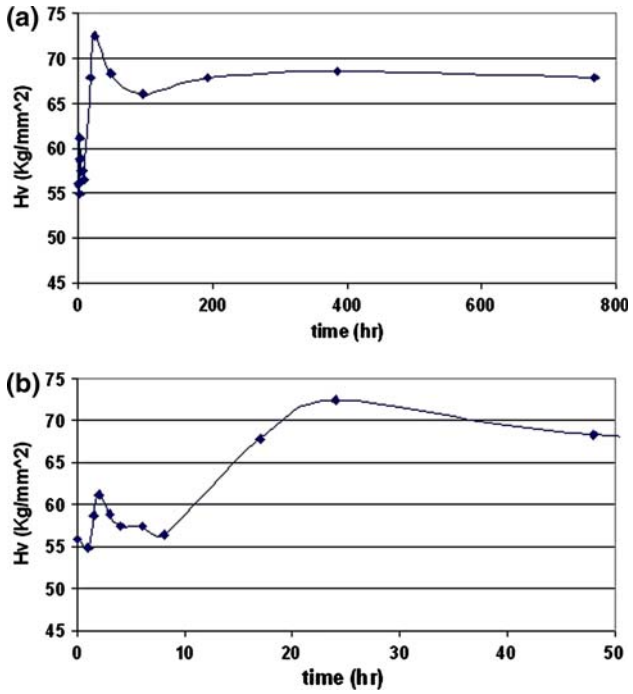

Fig. 5 Vickers hardness after aging at 225 °C for (**a**) 32 days, (**b**) the first 50 h

Solution treatment

Most of the phases composing the alloy were dissolved into the α-Mg phase, and only a few (about 0.5%area) Mg_2Sn precipitations (size up to 5μm) remained after the solution treatment. XRD analysis and EDS measurements confirmed that the only phases present after the solution treatment are α-Mg and Mg_2Sn.

Precipitation hardening

Solution treated samples were aged at 225 °C for different periods of time up to 32 days. Figure 5a, b show the Vickers hardness for the complete aging period and for the first 48 h, respectively. These values were taken using a 1 kg load on the Vickers' hardness indenter. Repeating this experiment using a 100 g load gave similar results.

Based on the hardness (Fig. 5a, b), it can be concluded that the investigated alloy is stable at elevated temperatures for at least 32 days. The hardness values become constant after 24 h of aging at 225 °C, and overaging did not occur during the entire testing period. The constant hardness is about 67 Hv (increase of 19.6% compared with the

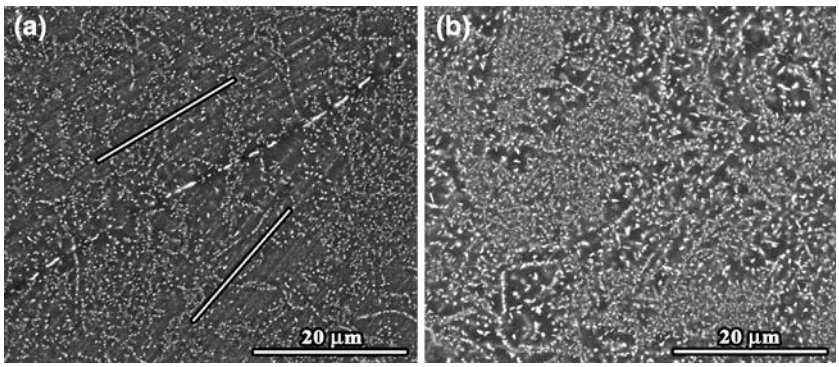

Fig. 6 SEM micrographs after aging at 225 °C for: (**a**) 1 day; (**b**) 32 days

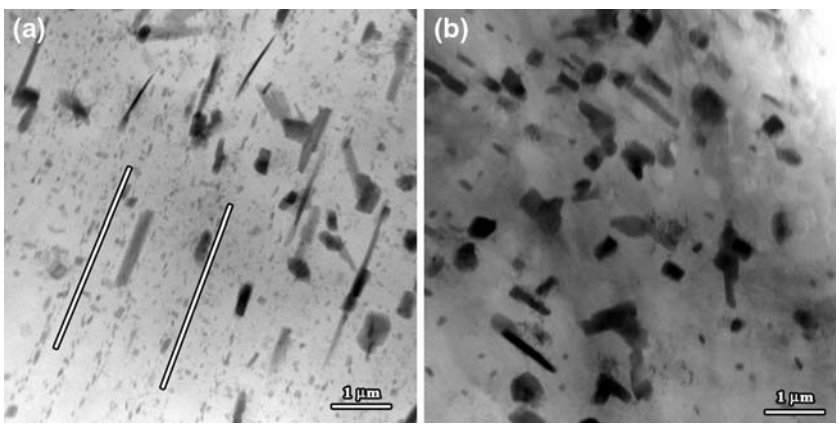

Fig. 7 STEM micrographs after (**a**) 1 day of aging, (**b**) 32 days of aging at 225 °C

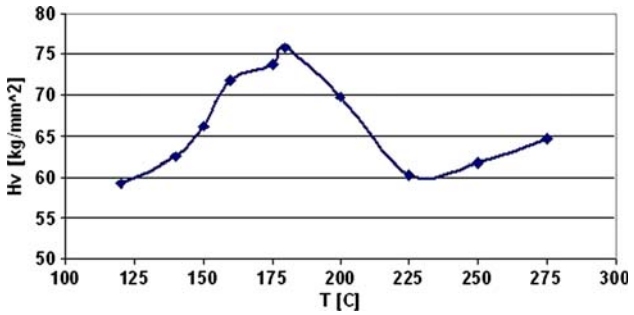

Fig. 8 Vickers hardness values vesus temperature after 2 h of aging

hardness of solution treated sample). Two hardness peaks are discernible—The first peak after 1 h and the second after 24 h. As shown before by HRTEM analysis [4, 5], the first peak is correlated to the precipitation of the $MgZn_2$ phase, whereas the second is correlated to the precipitation of the Mg_2Sn phase. Current EDS (in STEM) measurements are in accord with this precipitation sequence, but it could not be verified by electron diffraction due to the very small size of the precipitations (Figs. 6 and 7).

STEM micrographs (Fig. 7 a–b) taken after aging reveal that the precipitates can be grouped into two populations—one less than ~1μm and the other less than ~100 nm. SAXS results reveal that the smaller precipitates have either spherical or needle-like shape, and that in the initial stages of aging they are aligned with respect to the matrix. The aligned phenomenon can also be seen after 1 day of aging in SEM (Fig. 6a) and STEM (Fig. 7a) micrographs. Based on [5, 9] it can be assumed that the precipitates are $MgZn_2$. According to SEM micrographs (Fig. 6a, b), these precipitates are uniformly distributed in the matrix without any change in the alloy's microstructure during aging, besides loosing their alignment (compare Fig. 6a, b).

In addition, SAXS results show that after 4 days of aging (the beginning of the constant hardness value of the alloys) the size of round particles (~48 nm) hardly changed with aging times. STEM bright field micrograph (Fig. 7b) shows that some of the precipitates' size remained below 100 nm. The dimensions of the needle-like precipitates are ~250 nm in length and ~25 nm in width (10:1 ratio). The mean grain size of the investigated alloy after aging was 78.1 ± 14.3μm. These findings confirm the assumption that the microstructure of the alloy is very stable, although the relatively high aging temperature, which explains the constant micro-hardness values.

Activation energy for aging

The variation of hardness after 2 h of aging at different temperatures is presented in Fig. 8. Two hardness slopes are discernible. Assuming an Arrhenius type formulation

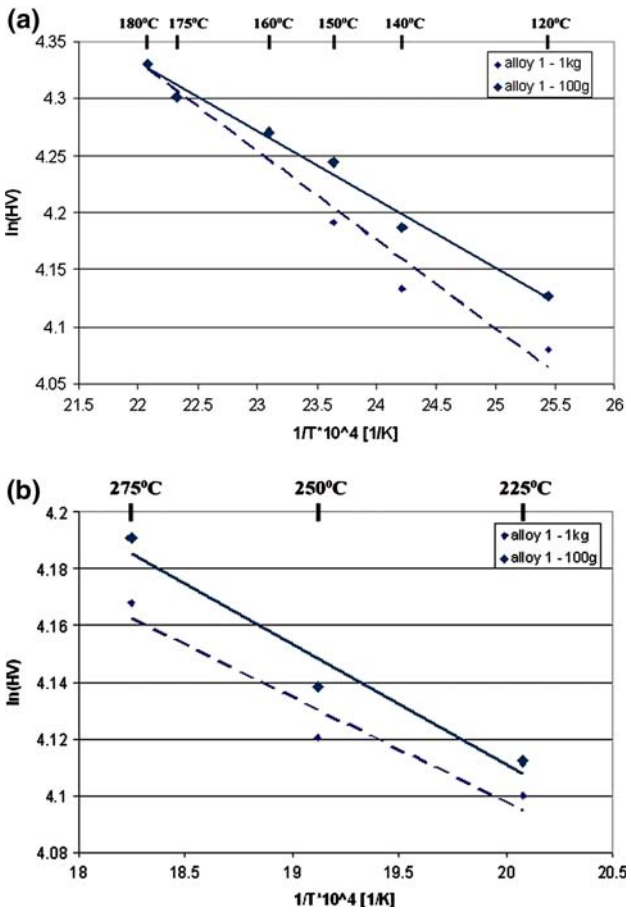

Fig. 9 Calculating the empirical activation energy related to the (**a**) first peak (**b**) second peak of the hardness process

for the dependence of the hardness on the aging temperature [10, 11], the empirical activation energy for each hardness peak was calculated from the slopes in Fig. 9a, b. The values are 5.7 kJ/mol and 3.3 kJ/mol, respectively.

Exposure to elevated temperature

As-cast samples were exposed to 225 °C for different periods of time up to 32 days. The hardness values (Fig. 10) are stable at about 59 Hv. SEM micrographs (Fig. 11 a, b) reveal very fine precipitates in the regions of high solutes content close to the grain boundaries. The fine precipitates show two morphologies, round and needle-like, similar to those in the aged samples. This fact indicates that the fine precipitates are the same as those found in the aged specimens, namely $MgZn_2$/MgZn and Mg_2Sn.

Discussion

The investigated alloy, Mg–5.6%Sn–4.4%Zn–2.1%Al has a fine microstructure: DAS of 17 μm as against 44 μm in

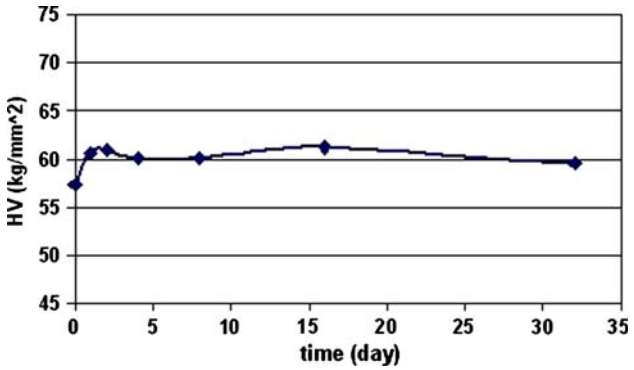

Fig. 10 Micro-hardness results during temperature exposure at 225 °C

the basic alloy [4, 5]. Furthermore, after solution treatment and aging, the mean grain size was 78 μm, which is smaller than that of typical gravity die cast Mg alloys [12]. Solution treatment at 450 °C dissolved uniformly most of the as-cast phases. The precipitate distribution after aging (Fig. 6) confirms this.

The two hardness peaks found during aging correspond with two types of precipitates found in the Mg–Sn–Zn base alloy, namely the precipitation of $MgZn_2$ followed by the precipitation of Mg_2Sn [4, 5]. This sequence resulted from the higher diffusion coefficient of Zn in Mg and the coherency between the $MgZn_2$ and the Mg matrix.

The $MgZn_2$ coherency with the matrix is also reflected in the alignment of the precipitates during the earlier stages of aging (Figs. 6a and 7a). SAXS measurements revealed that these particles are either round (mean size of ~48 nm) or plate-like (mean length of ~250 nm) throughout the complete test period of 32 days. This explains the constant high hardness found in the addressed alloy as against rapid overaging observed in the Al-free base alloy.

The different hardening mechanisms, i.e., the two types of precipitates responsible for hardening, find their expression in the two distinct activation energies found at low and high temperatures. At low temperatures and after 2 h of aging, only $MgZn_2$ precipitates exist, hence the activation energy in this temperature range (5.7 kJ/mole) corresponds to this type of precipitates. At higher temperatures, the precipitation of Mg_2Sn determines the hardness, hence its activation energy is 3.3 kJ/mole. The value for the precipitation of $MgZn_2$ is close to the one found for Mg–Ca–Zn [10] and ZA84 Mg–alloy [12]. Since the activation energy for bulk diffusion of Zn in Mg is 120 kJ/mole and for Sn it is 150 kJ/mole [13], it can be concluded that the precipitation is grain boundary diffusion-dependent rather than bulk diffusion dependent.

The benefit of adding 2%wtAl is quite obvious; compared with the Al-free base alloy the Al addition seems to slow down the precipitation of $MgZn_2$ and Mg_2Sn. Therefore, the hardness peaks in the investigated alloy took place after 1 h and 24 h, whereas for the basic alloy only the second peak was discernible after aging for 1 h at 225 °C, and overaging took place already after 16 h [4]. The slow precipitation can be attributed to the presence of Al at the precipitate/matrix interface or to the fact that the Al atoms dissolved in the α-Mg matrix serve as a diffusion barrier to the Sn and Zn atoms.

The addition of Al, at the low level examined in the current study, resulted in Mg and $Mg_{32}(Al,Zn)_{49}$ eutectic rather than Mg and MgZn, which was found in Mg–Sn–Zn base alloy [5]. This is in accord with the formation of τ-$Mg_{32}(Al,Zn)_{49}$ in Mg–Zn–Al alloys with a Zn:Al ratio of about 2:1 [12]. The formation of the apparently more stable $Mg_{32}(Al,Zn)_{49}$ suppressed the formation of γ-$Al_{12}Mg_{17}$, which soften at elevated temperatures and hence is deleterious for applications at elevated temperatures. Therefore, Mg–5.6%Sn–4.4%Zn–2.1%Al, which exhibits stable structure and mechanical (hardness) properties at 225 °C, is a very promising Mg–alloy for high temperature applications.

Conclusions

- The investigated alloys show stable microstructure that is reflected in stable hardness values at 225 °C for 32 days.

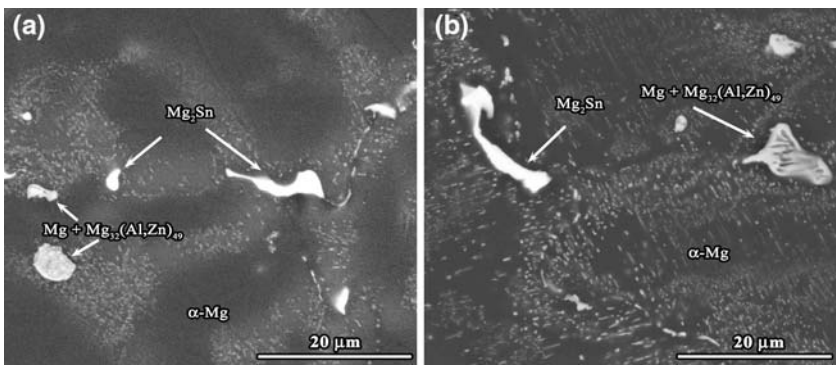

Fig. 11 SEM micrographs after exposure to 225 °C for (**a**) 1 day; (**b**)32 days

- The eutectic is composed of Mg and $Mg_{32}(Al,Zn)_{49}$ rather than Mg and MgZn found in Mg–Sn–Zn alloys.
- γ-$Mg_{17}Al_{12}$ phase does not form because Al is consumed by the $Mg_{32}(Al,Zn)_{49}$ phase.
- Al addition delayed the precipitation of $MgZn_2$ and Mg_2Sn, in comparison with Al-free Mg–Sn–Zn alloys.
- The investigated Mg–Zn–Sn–Al alloy is a promising candidate for future commercial applications at elevated temperatures.

References

1. Regev M, Rosen A, Bamberger M (1999) In: Froes FH, Ward-Close CM, Eliezer D, McCormick P (ed) Synthesis of lightweight metals III, TMS 163
2. Zhang Z, Couture A (1998) Scripta Mater 39:45
3. Blum W, Zhang P, Watzinger B, Grossmann BV, Haldenwanger H (2001) Mater Sci Eng A319–321:735
4. Cohen S, Goren-Muginstein GR, Abraham S, Dehm G, Bamberger M (2004) In: Luo AA (ed) Mg Technology 2004, TMS 2004 annual meeting, Charlotte, USA, 14–18 March 2004, p 301
5. Cohen S, Goren-Muginstein G, Avraham S, Rashkova B, Dehm G, Bamberger M (2005) Zeitschrift für Metasllkunde 96:1081
6. Horie T, Iwahori H, Seno Y, Awano Y (2000) In: Kaplan HI, Hyrn JN, Clow BB (eds) Mg Technology 2000, TMS 2000 annual meeting, Nashville, USA, 12–15 March 2000, p 261
7. Maeng D, Kim T, Lee J, Hong S, Seo S, Chun B (2000) Scripta Mater 43:385
8. Massalski T (1992) Binary alloy phase diagrams, 2nd edn. ASM Int
9. Gorny A, Katsman A, Popov I, Bamberger M (2007) In: Beals RS, Lou AA, Neelameggham NR, Pekguleryuz MO (eds) Mg Technology 2007, TMS 2007 annual meeting, Orlando, USA, 26 February, 1 March 2007, p 307
10. Reed-Hill RE, Abbaschian R (1992) Physical metallurgy principles. PWS-KENT Publishing Co., Boston, MA, USA, pp 677–678
11. Bamberger M, Levi G, Vander Sande JB (2006) Metall Mater Trans A 37:481
12. Wang Y, Guan S, Zeng X, Ding W (2006) Mater Sci Eng A416:109
13. Smithells CJ (1970) Metals reference book, 5th edn